MECH 498: Research Practicum

Final Paper

Spring 2022

Word Count: 2498

The Role of the Nucleus in Collective Cell Migration

Brady Hine
Colorado State University
Mechanical Engineering Department
School of Biomedical Engineering
Fort Collins, CO 80523

Dr. Soham Ghosh
Colorado State University
Mechanical Engineering Department
School of Biomedical Engineering
Fort Collins, CO 80523

ABSTRACT

Cell migration is a fundamental process in normal physiology and pathology. The cell nucleus is emerging as a key mediator in this process [1,2]. Being the largest and stiffest organelle in eukaryotic cells, the nucleus acts as a defining factor during cell migration. The role of nuclear mechanics in cell migration is therefore a topic of recent interest to both the basic science and clinical research communities. The objective of the proposed work is to study how nuclear mechanical properties affect collective cell migration using a model system of the scratch wound assay of fibroblasts. Quantitative understanding of collective cell migration will be obtained using live time lapse imaging of cells with modified nuclear stiffness and altered chromatin remodeling modalities.

1 Introduction

To quantitatively assess the role of the nucleus in collective cell migration, it is important to understand the trajectory of single cells in the context of collective cell migration, and to decide on some parameters to quantify the trajectory of migration. In the migration mode of cell crawling, visualized in figure 1, cells generally move in response to external chemical or physical signals in the environment detected by focal adhesions connected to the cytoskeleton [3]. During this, the actin cytoskeleton is generally referred to as the engine of motility due to its elaborate network driving the first step of cell movement through protrusion using forces generated from asymmetric polymerization. When there's a group, sheet, or chain of these cells moving together, there are additional forces due to cell-cell adhesion effects via adherens-junction proteins coupled to the cytoskeleton increasing complexity compared to single cell migration [4]. These junctions connect cells to their neighbors allowing for both chemical and mechanical communication and is attributed to why collective migration is observed to be faster and more efficient than cells migrating individually [5]. It's known that the wound healing response of cells decreases with aging. Aging is associated with increase in genomic instability, characterized by the softening of the nucleus and a condensing of the chromatin structure as shown in figure 1 [6,7]. To investigate how such changes in the mechanics

of the cell nucleus and chromatin architecture affect the collective cell migration, a scratch wound assay model was used in the present study. The scratch wound assay is a simple and well-established technique to quantify some standard collective cell migration parameters such as speed and persistence of migrating cells [8]. In the model, a sheet of cells is scratched with a pipette tip causing the cells to move perpendicular to the wound to seal it as visualized in figure 1. This begins the migration process from a defined starting point and allows the use of time-lapse imaging and image processing to capture speed and directional persistence of cell migration. NIH-3T3 mouse embryonic fibroblast cells were used in this study because they are an excellent model system for this assay, relevant to many connective tissues.

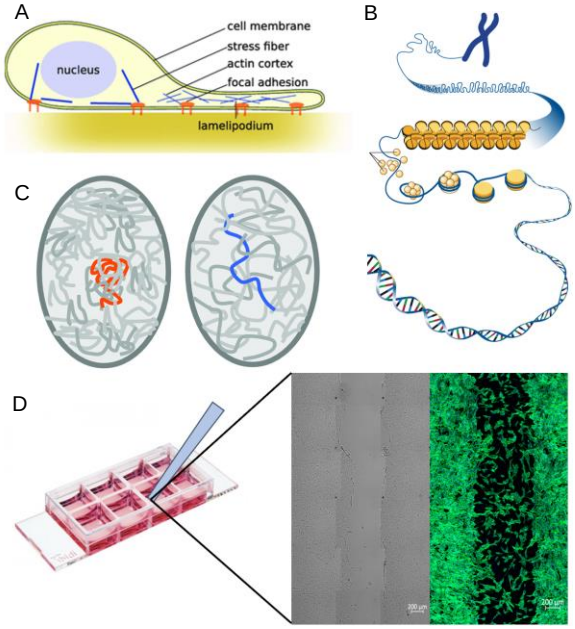

Figure 1. (A) Visualization of single cell crawling in 2D [9]. (B) Chromosome structure showing a chromatin fiber, histones, nucleosomes, and DNA [10]. (C) Depiction of condensed chromatin (left) illustrating GSK126 treatment and decondensed chromatin (right) [11]. (D) Depiction of the scratch wound assay model.

2 Materials and Methods

2.1 Scratch Wound Assay

The scratch wound assays performed in this study were conducted using an ibidi® 8 well µ-Slide plate (Cat no: 80826). In order to functionalize these plates for cell attachment, the wells were first plasma treated for a few seconds before the application of a collagen solution (Gibco A10664). This solution was left for at least 30 minutes allowing for a collagen layer to form. After this, NIH-3T3 cells were seeded into the wells and provided with the fibroblast specific medium (ATCC 30-2022) supplemented with Pen/Strep (Gibco 15140-122) and FBS (Gibco 261-40-079). After an incubation period of 48 hours, cell layer confluency was observed, and a scratch was applied on the cell monolayer using a 200µL pipette tip guided by a straightedge. Next, the wells were quickly rinsed with 1X phosphate buffered saline (PBS) and provided with a fresh fibroblast specific medium.

2.2 Migration Imaging

All imaging was done using a Zeiss LSM 980 inverted confocal microscope. Both brightfield and stained cell images were captured using live and fixed staining techniques. Live staining was done using NucBlue (Thermo Fisher) while fixed staining was done using DAPI (Thermo Fisher) and phalloidin (Thermo Fisher), post permeabilization of the cell membrane using Triton. For live imaging, the 8 well slides were placed inside the microscope with a sufficient amount of culture medium. We maintained a physiologically relevant temperature (37° C), CO_2 concentration (5%), and humidity level. Tile regions were defined in the microscope surrounding the applied scratch in each well with time intervals set between images taken. During the imaging process, as some medium would aspirate, fresh medium would occasionally be added to reduce risks of the cells drying out.

2.3 Altering Chromatin and Nuclear Mechanics

As mentioned in the introduction, we were interested to find how changes to the chromatin architecture and nuclear mechanics would affect the wound healing collective cell migration process. To induce changes in the chromatin architecture, GSK126 (Sigma) was applied to some treatment groups at a concentration of 20µM 24 hours prior to scratch application and again in media supplied post-scratch. GSK126 is an EZH2 methyltransferase inhibitor which has been used in previous studies to inhibit chromatin remodeling [12]. For inducing changes to the nuclear mechanics, Trichostatin A (TSA) (Sigma) was applied using

a similar approach at a concentration of 100ng/ml. TSA is a class I and II histone deacetylase inhibitor which has been used previously to induce a decrease in cell nuclear stiffness [13].

2.4 Image Processing

Most image processing was done using the open source software Fiji [14]. First, the percentage wound closure at given time points were calculated. This was done by outlining a region of interest (ROI) of the initial scratch in brightfield images and calculating an area measurement serving as A_0. At a later timepoint, the number of cells within the initial wound area was counted (n) and the average cell area of 5 cells was recorded (A_c) and multiplied by n to get a closed area measurement A_t as shown in equation 1. The percent wound closure was then calculated as seen in equation 2.

$$A_t = n * A_c \quad (1)$$

$$\%WC = \frac{A_t}{A_0} * 100 \quad (2)$$

In order to collect cell specific migration parameters such as migration speed, the Fiji plugin TrackMate was used with live NucBlue stained images [15]. These were converted to a binary mask allowing for the plugin to perform a spot detection on frames and link the paths these spots followed throughout the migration into tracks. These tracks allowed for the calculation of parameters including total distance travelled, mean speed, and linearity of forward progression shown in equations 3-5 respectfully [15].

$$total\ distance\ traveled = \sum_i d_{i,i+1} \quad (3)$$

$$mean\ speed = \frac{total\ distance}{total\ time} \quad (4)$$

$$linearity\ of\ forward\ progression = \frac{total\ time * mean\ speed}{net\ distance} \quad (5)$$

3 Results

3.1 Wound Closure Analysis

When performing the wound closure analysis, brightfield images were taken at 30-minute intervals for control, GSK, and TSA groups over a 25.5 hour timespan. All groups underwent the experiment simultaneously with two control samples, 3 GSK samples, and 3 TSA samples. The visual results for this experiment can be seen in figure 2 below.

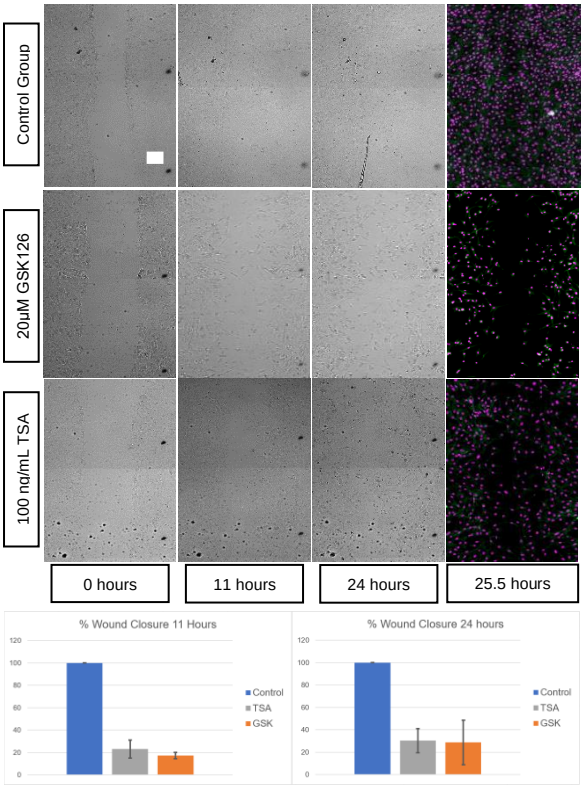

FIGURE 2. (Top) Migration images for control, GSK126, and TSA groups from 0-25.5 hours with final fixed images stained for nuclei in purple and actin in green. Scale bar 100μm. (Bottom) Wound closure percentage graphs of groups at 11 and 24 hours showing a significant decrease for the TSA and GSK126 treatments. Error bars show standard deviation about the mean with (n = 3) samples.

Wound closure percentage measurements were taken at 11 and 24 hour timepoints as described previously with the 11 hour timepoint chosen as this is when full closure of the control wound was observed. The results showed a significant decrease ($p<0.05$) in the wound closure percentage of the GSK and TSA groups when compared to the control using two sample t-tests.

3.2 Live Nuclear Stained Analysis

The scratch wound assay was repeated for the treatment groups but prior to imaging, the cell nuclei were stained using NucBlue. This imaging took place between 2-8.5 hours after scratch application as this seemed like a decent window to observe migration from results in section 3.1. Similarly, all groups underwent the experiment simultaneously with two control

samples, 3 GSK samples, and 3 TSA samples. Images were again taken at 30-minute intervals with initial brightfield images, followed by stained images shown below in figure 3.

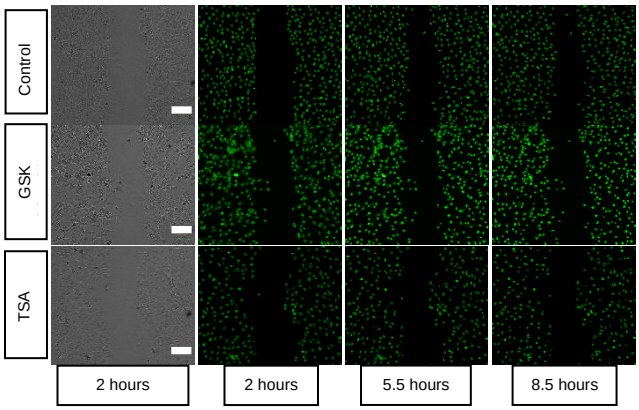

Figure 3. Scratch wound assay images in brightfield and live stained for the nucleus from 2-8.5 hours post scratch. Scale bar is 100µm.

These migration images seemed to have similar trends as our previous results from a qualitative analysis. The staining used here allowed for observations of the nuclear structure with an apparent condensing of the nucleus seen throughout the GSK treatment group. This migration data was then processed through TrackMate image processing as described in section 2.4. A visualization of the tracks generated, and spot detection can be seen in figure 4 for the start and endpoints of the migration.

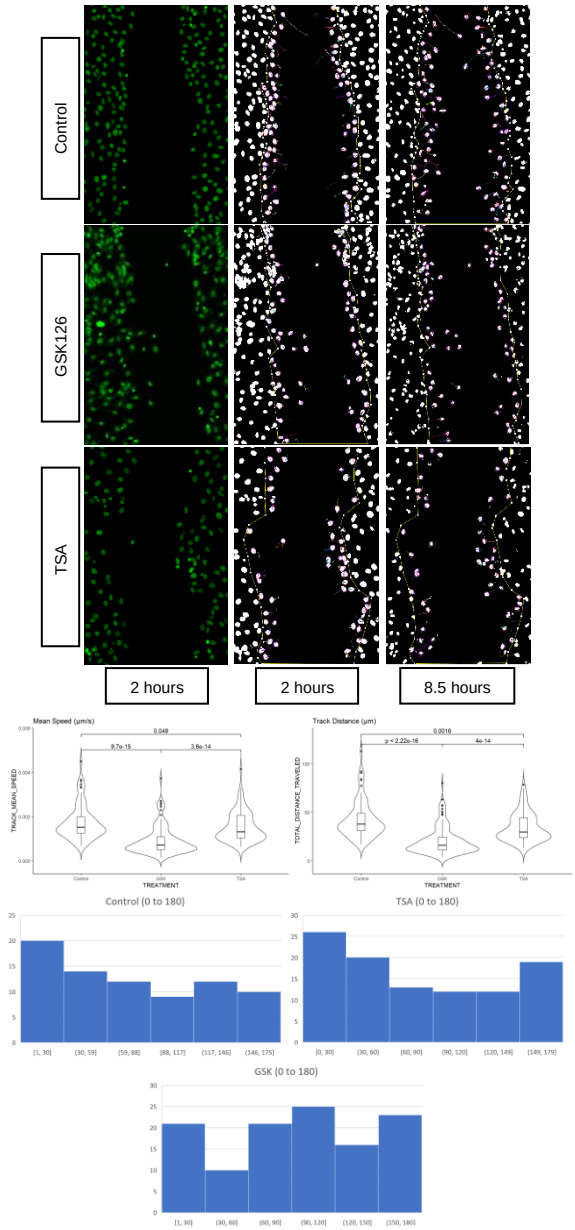

Figure 4. (Top) TrackMate path visualization for cells migrating in figure 4. (Middle) Violin plots for the mean speed and track distance of migrating cells at the wound edge. TSA shows a small decrease in speed and distance while GSK126 drastically decreased speed and distance. (n > 73) cells tracked for each group. (Bottom) Angular trajectory histograms of migrating cells between groups in a 0-180 degree format. GSK shows a more random distribution.

From the data gathered with TrackMate, violin plots were generated using RStudio for the mean migration speed and overall distance travelled by the migrating cells [16]. Significance between groups was determined using a one-way ANOVA (followed by post hock test) with a ($p<0.05$) indicating statistical significance. From

the plots it was seen that TSA treatments had a significant reduction in both the migrating speed and distance travelled by the cells. This reduction was seen to be even more drastic for the GSK treatments for both parameters.

3.3 Angular Trajectory Analysis

When investigating migration parameters as described in section 3.2, it was found that there was no difference between the linearity of forward progression for the migrating cells between treatments. While this measure provides insight into how straight of a path the cells take, it doesn't reveal much about the migration as even random walks can be seen as persistent. To further investigate if there were differences in migration trajectory between the treatment groups, a different approach was used for this data. Here, each side of the wound was manually investigated using TrackMate to collect initial and final coordinates of the cells as x_1,y_1 and x_2,y_2 respectively. For ease of processing the data, the left side of the wound served as the baseline orientation so when collecting data for the right side of the wound, the images were first flipped over the vertical axis. These coordinates were then used to quantify a theta (θ) relative to the horizontal of each cell for their migration path from the wound edge using equation 6.

$$\theta = \tan^{-1}\frac{y_2 - y_1}{x_2 - x_1} \quad (6)$$

The thetas generated from this equation were given in a format of -180 to 180 degrees and so, for ease of data interpretation, an absolute value was taken. The thetas could then be interpreted with low angles corresponding to a more direct migration into the wound with larger angles corresponding to less directed migration toward wound healing. Theta distributions can be seen for each treatment group in figure 4. For the control, GSK, and TSA groups, theta means were 77.5° (53.9°), 94.0° (52.9°), and 80.7° (55.8°) respectfully with standard deviations given in parentheses. Using two sample t-tests between the groups, it was found that the thetas for GSK groups were statistically ($p<0.5$) larger than those of the control and TSA groups with no statistical difference between the latter.

3.4 Qualitative Actin Structure Comparison

Next, we asked the question, how the angular values of trajectory were affected by the treatment groups and we investigated actin structure between the different treatment groups because actin structure is known to be the key mediator of migration. This was investigated using the fixed phalloidin stained images from section 3.1 and a comparison of high-resolution images were performed. The results are shown in figure 5 below.

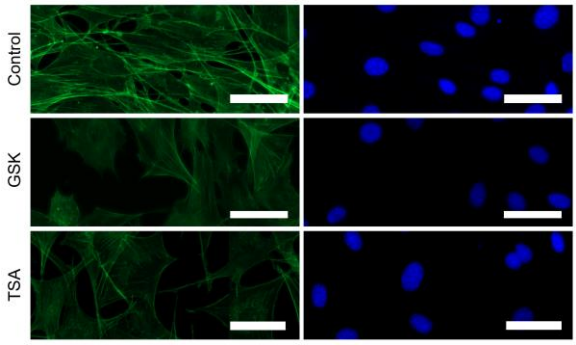

Figure 5. High resolution fixed stained images of the actin (left) and nuclei (right) of the treatment groups. Scale bar is 50μm.

While there were differences seen in the overall cell shape between the groups, they all exhibited the fibrous F-actin structure characteristic of actin cytoskeleton. This provided evidence that the differences of angular trajectory as described in prior sections of the results was not caused by a breakdown of the actin structure for either the TSA or GSK treatments.

4 Discussion

The results described in this paper showed that the nucleus indeed plays an important role in collective cell migration. Softening the nucleus, by TSA application, and condensing the chromatin architecture, by GSK application, were decreased the wound healing ability of cells in the scratch wound assay model. Part of this change was a noticeable decrease in the migration speed with TSA with an even more drastic decrease seen with GSK treatment.

A very interesting finding in this study was that the GSK treatment seemed to interrupt the ability of cells to follow migration gradients during the wound healing process which wasn't seen with TSA. This could be seen by the much

larger variation of theta in this group compared to the others possibly signaling a breakdown in the cell-cell wound healing communication. As actin is generally the engine of motility for migrating cells, we wanted to see whether the GSK treatments were inducing any noticeable changes in the actin cytoskeleton structure. From a qualitative perspective, this did not seem to be the case, providing evidence that the condensed chromatin structure is limiting the cell migration through a different manner exclusive to the nucleus. The exact mechanism behind this was not able to be fully investigated in the context of this study and needs further investigation.

5 Conclusion

In this study, we investigated how modifications to the nuclear mechanics and chromatin structure can affect collective cell migration. It was found that nuclear softening via TSA, and chromatin condensing via GSK126 both had a negative impact on the migration and wound healing of NIH-3T3 murine fibroblasts. The effects of GSK126 appeared to be more unfavorable for migration and the cells exhibited a limited ability to follow migration gradients which wasn't observed in other groups. This study lays the foundation for future work aimed at targeting these mechanisms in reverse to increase the migration and wound healing ability of aged cells.

REFERENCES

[1] S. Jain et al., "The role of single-cell mechanical behaviour and polarity in driving collective cell migration," Nat. Phys. 2020 167, vol. 16, no. 7, pp. 802–809, May 2020, doi: 10.1038/s41567-020-0875-z.

[2] D. M. Graham et al., "Enucleated cells reveal differential roles of the nucleus in cell migration, polarity, and mechanotransduction," J. Cell Biol., vol. 217, no. 3, pp. 895–914, Mar. 2018, doi: 10.1083/JCB.201706097.

[3] C. De Pascalis and S. Etienne-Manneville, "Single and collective cell migration: the mechanics of adhesions," https://doi.org/10.1091/mbc.e17-03-0134, vol. 28, no. 14, pp. 1833–1846, Oct. 2017, doi: 10.1091/MBC.E17-03-0134.

[4] F. Thüroff, A. Goychuk, M. Reiter, and E. Frey, "Bridging the gap between single-cell migration and collective dynamics," Elife, vol. 8, Dec. 2019, doi: 10.7554/ELIFE.46842.

[5] R. Mayor and S. Etienne-Manneville, "The front and rear of collective cell migration," Nat. Rev. Mol. Cell Biol. 2016 172, vol. 17, no. 2, pp. 97–109, Jan. 2016, doi: 10.1038/nrm.2015.14.

[6] Purohit, Jogeswar Satchidananda, and Madan Mohan Chaturvedi. "Chromatin and Aging." Topics in Biomedical Gerontology 205–241. 18 Aug. 2016, doi:10.1007/978-981-10-2155-8_11

[7] Phillip, Jude M et al. "The Mechanobiology of Aging." Annual review of biomedical engineering vol. 17 (2015): 113-141. doi:10.1146/annurev-bioeng-071114-040829

[8] Liang, CC., Park, A. & Guan, JL. In vitro scratch assay: a convenient and inexpensive method for analysis of cell migration in vitro. Nat Protoc 2, 329–333 (2007). doi:10.1038/nprot.2007.30

[9] Antoine Fruleux and Rhoda J Hawkins 2016 J. Phys.: Condens. Matter 28 363002

[10] NIH. "Chromatin." National Human Genome Research Institute (2022).

[11] Spagnol ST, Dahl KN. "Spatially Resolved Quantification of Chromatin Condensation through Differential Local Rheology in Cell Nuclei Fluorescence Lifetime Imaging." PLOS ONE 11(4): e0154639 (2016). doi:10.1371/journal.pone.0154639

[12] Kaur, Jasmine et al. "Targeting Chromatin Remodeling for Cancer Therapy." Current molecular pharmacology vol. 12,3 (2019): 215-229. doi:10.2174/1874467212666190215112915

[13] Fischer, Tony et al. "Effect of Nuclear Stiffness on Cell Mechanics and Migration of Human Breast Cancer Cells." Frontiers in cell and developmental biology vol. 8 393. 29 May. 2020, doi:10.3389/fcell.2020.00393

[14] Schindelin, J., Arganda-Carreras, I., Frise, E., Kaynig, V., Longair, M., Pietzsch, T., … Cardona, A. (2012). Fiji: an open-source platform for biological-image analysis. Nature Methods, 9(7), 676–682. doi:10.1038/nmeth.2019

[15] Ershov, D., Phan, M.-S., Pylvänäinen, J. W., Rigaud, S. U., Le Blanc, L., Charles-Orszag, A., … Tinevez, J.-Y. (2021, September 3).

Bringing TrackMate into the era of machine-learning and deep-learning. Cold Spring Harbor Laboratory. doi:10.1101/2021.09.03.458852
[16] RStudio Team (2020). RStudio: Integrated Development for R. RStudio, PBC, Boston, MA URL http://www.rstudio.com/